
Reproducibility of Regional Metabolic Covariance Patterns: Comparison of Four Populations

James R. Moeller, Toshitaka Nakamura, Marc J. Mentis, Vijay Dhawan, Phoebe Spetsieris, Angelo Antonini, John Missimer, Klaus L. Leenders and David Eidelberg

Department of Psychiatry, Columbia College of Physicians and Surgeons, New York; New York University School of Medicine, New York; Functional Brain Imaging Laboratory, North Shore University Hospital, Manhasset, New York, New York; and Paul Scherrer Institute, Villigen, Switzerland

In a previous [¹⁸F]fluorodeoxyglucose (FDG) PET study we analyzed regional metabolic data from a combined group of Parkinson's disease (PD) patients and healthy volunteers (N), using network analysis. By this method, we identified a unique pattern of regional metabolic covariation with an expression which accurately discriminated patients from healthy volunteers. To assess the reproducibility of this pattern as a potential marker for PD, we compared the pattern's topography with that of the disease-related covariance patterns identified in three other independent populations of patients with PD and healthy individuals studied in different PET laboratories. **Methods:** The following patient populations were studied: group A (original cohort: 22 PD, 20 N; resolution: 7.5 mm full width at half maximum [FWHM]); group B (18 PD, 12 N; resolution: 4.2 mm FWHM); group C (25 PD, 15 N; resolution: 8.0 mm FWHM); and group D (14 PD, 10 N; resolution: 10 mm FWHM). Region weights for the PD-related covariance pattern (PDRP) identified in the group A analysis were correlated with those for the disease-related patterns identified in the analyses of groups B, C and D. In addition, subject scores for the group A PDRP were computed prospectively for every individual in each of the study populations. PDRP scores for PD and N within each cohort were compared. **Results:** The PDRP topography identified in group A was highly correlated with each of the corresponding topographies identified in the other populations ($r^2 \sim 0.60$, $P < 0.0001$). Prospectively computed subject scores for the group A PDRP significantly discriminated PD from N in each population ($P < 0.004$). **Conclusion:** The PDRP topography identified previously in Group A is highly reproducible across patient populations and tomographs. Prospectively computed PDRP scores can accurately discriminate patients from controls in multiple populations studied with different tomographs. Brain network imaging with FDG PET can provide robust metabolic markers for the diagnosis of PD.

Key Words: regional metabolic covariance patterns; FDG PET, Parkinson's disease

J Nucl Med 1999; 40:1264–1269

The authors have used the scaled subprofile model (SSM) (1–3) extensively in the study of Parkinson's disease

Received Jul. 13, 1998; revision accepted Jan. 12, 1999.

For correspondence or reprints contact: David Eidelberg, MD, Functional Brain Imaging Laboratory, North Shore University Hospital, 350 Community Dr., Manhasset, New York, 11030.

(PD), a common akinetic-rigid movement disorder. In our previous PET studies with ¹⁸F-fluorodeoxyglucose (FDG), we identified a specific pattern of regional metabolic covariation associated with PD (4,5). This covariance pattern was characterized by relative hypermetabolism of the lentiform nucleus and thalamus, associated with metabolic decreases in the primary and association motor cortices. We have shown that subject scores for this PD-related covariance pattern (PDRP) representing its expression in individual patients, correlate significantly with independent measures of clinical disability as measured by the Unified Parkinson's Disease Rating Scale (4,6,7). Moreover, PDRP subject scores correlate with presynaptic nigrostriatal dopaminergic function as measured by striatal uptake of [¹⁸F]fluorodopa (FDOPA) (5) and with changes in motor performance after stereotactic pallidotomy (8).

We have also developed a technique for computing the expression of this network in individual subjects. This algorithm is referred to as the topographic profile rating (TPR) (7) and is used to compute subject scores for the original PDRP (4) on a prospective individual scan basis (9,10). Indeed, in PD, these measures of network expression are predictive of independent measures of clinical disability (7). In parallel studies, we also found that subject scores for a related covariance pattern of regional metabolic asymmetries can differentiate early stage PD patients from healthy individuals with an accuracy comparable with FDOPA PET (5,11). Moreover, using the TPR algorithm, subject scores for this pattern accurately distinguished drug-responsive from drug-resistant parkinsonians at the earliest stages of disease (11). These findings suggest that quantifying the expression of the PDRP in individual subjects can assist in the early differential diagnosis of parkinsonism and may also provide an objective measure of disease progression.

For the PDRP to serve as a useful metabolic marker of parkinsonism, this metabolic topography must be reproducible across patient populations and PET instruments. In this study, we examined PDRP reproducibility by comparing its topography with that of each of the disease-related metabolic covariance patterns identified in separate SSM analyses of metabolic data from three other independent PD patient populations scanned in different laboratories with

PET tomographs of varying resolution and sensitivity. We also used TPR to compute PDRP scores for the subjects in each population on a prospective case basis. We compared PDRP expression in patients and controls across the study populations.

MATERIALS AND METHODS

Subjects

The following four populations were studied with quantitative FDG PET.

Group A. Twenty-two PD patients (57.9 ± 11.4 y; mean \pm SD) and 20 healthy volunteers (47.0 ± 17.1) were scanned with FDG PET using the SuperPETT3000 tomograph (Scanditronix, Essex, MA) at North Shore University Hospital, Manhasset, NY (12), with an axial resolution of 7.5 mm full width at half maximum (FWHM). Images were reconstructed with an 8-mm filter. The clinical and metabolic data from this group have been reported previously (4).

Group B. Eighteen PD patients (55.2 ± 6.0 y) and 12 healthy volunteers (54.6 ± 9.2 y) were scanned with FDG PET using the General Electric Advance tomograph (General Electric, Milwaukee, WI) at North Shore University Hospital (13), with an axial resolution of 4.2 mm FWHM. Images were reconstructed with a 6-mm filter. The PD patients in this group were divided into two cohorts: subgroup B1, with 8 PD patients (54.9 ± 7.4 y) with early stage disease (Hoehn and Yahr stage I); and subgroup B2, with 10 PD patients (55.4 ± 5.1 y) with more advanced disease (Hoehn and Yahr stages III and IV, mean stage 3.2 ± 0.4). Limited clinical and metabolic data from this subgroup have been reported previously (14,15).

Group C. Twenty-five PD patients (57.8 ± 8.9 y) and 15 healthy volunteers (61.3 ± 10.9 y) were scanned with FDG PET using the ECAT 933-16 tomograph (CTI/Siemens, Knoxville, TN) at Paul Scherrer Institute, Villigen, Switzerland (16), with an axial resolution of 8.0 mm FWHM. Images were reconstructed with an 8-mm filter.

Group D. Fourteen PD patients (49.1 ± 12.0 y) and 10 healthy volunteers (27.2 ± 5.1 y) were scanned with FDG PET using the PC4600 tomograph (Cyclotron Corp., Berkeley, CA) at Memorial Hospital, New York, NY (17), with an axial resolution of 10 mm FWHM. Images were reconstructed with a 12-mm filter. Clinical and metabolic data from this group were reported previously (5).

Metabolic Covariance Analysis

Pattern Reproducibility. Similar quantitative FDG PET methods were used to calculate global and regional rates of glucose metabolism (rCMRGlc) in all patients and control groups (4,5,16). These scans were performed with subjects fasting; all antiparkinsonian medications were discontinued at least 12 h before the imaging procedures. rCMRGlc values for 30 standardized regions of interest (ROIs) were computed in each patient, as reported previously (4,14). In each population, SSM analysis was used to identify a disease-related pattern with an expression in individual subjects (subject scores) that discriminated PD patients from healthy volunteers. In these SSM analyses, we used combined rCMRGlc data from PD patients and healthy volunteers (1-4). In each population, a disease-related pattern was identified such that its subject scores discriminated the patients from healthy volunteers at $P < 0.001$ (F-test according to Wilks λ). In each SSM analysis, the disease-related pattern was represented by either the

first or second principal component or a linear combination of both. Region weights for the PDRP identified in group A (4) were correlated with corresponding region weights for the disease-related covariance patterns identified in the separate SSM analyses of the FDG PET metabolic data from groups B, C and D. These region weight correlations were performed by computing Pearson product moment correlation coefficients. Correlations were considered significant at $P < 0.05$.

Voxel-Based Covariance Analysis. A voxel-based approach was also used to identify a disease-related pattern without the placement of manual ROIs. SSM was applied on a voxel-by-voxel basis to the group B scan data. (We chose group B scans for this analysis because of the greater field of view of the PET camera used in this population, which allowed the acquisition of data from the whole brain). FDG PET scans were placed in Talairach space and smoothed (10×10 mm) in axial, sagittal and coronal planes using statistical parametric mapping (18) on a personal computer (PC) platform running Windows NT (Microsoft, Seattle, WA) and MATLAB 5.0 (Mathworks, Inc., Natick, MA). SSM was applied to the smoothed, normalized images using algorithms written in programming language C on the same PC, Windows NT platform. A disease-related voxel-based covariance pattern was identified analogous to that in the ROI analysis. Subject scores for the ROI and voxel-based patterns were compared using correlational analysis as described above.

Prospective Discrimination. In subsequent analyses, the group A PDRP was used as a metabolic marker for parkinsonism, using the TPR algorithm (7,9). Region weights for the disease-related pattern identified in group A were projected prospectively into the rCMRGlc data from each member of groups B, C and D to compute individual subject PDRP scores. The TPR computational procedure was performed in an automated blinded fashion as described previously (7,9-11,15). In each population, the computed PDRP scores for the PD patients and the healthy volunteers were compared, using discriminant analysis (F-test according to Wilks λ). In addition, in each population, the computed PDRP scores for the patients and healthy volunteers were correlated with the corresponding subject scores for the disease-related pattern identified in the SSM analysis of each group's rCMRGlc data. The results of the discriminant analysis of the PDRP scores and the correlational analysis of the subject scores were considered significant at $P < 0.05$.

RESULTS

Pattern Reproducibility

In all four groups, SSM analysis of rCMRGlc data from PD patients and healthy volunteers disclosed PDRPs of similar topography (Fig. 1). The patterns were characterized by relative hypermetabolism of the basal ganglia and thalamus covarying with metabolic decreases in lateral frontal and paracentral motor areas and in the parieto-occipital association cortex. Region weights for the disease-related patterns identified in the analyses of groups B, C and D correlated significantly with corresponding regional values for the original group A PDRP ($r^2 > 0.58$, $P < 0.001$) (Fig. 2). In addition, significant pairwise correlations were noted between the region weights for the disease-related covariance patterns identified in the SSM analyses of groups B, C and D ($r^2 > 0.51$, $P < 0.001$).

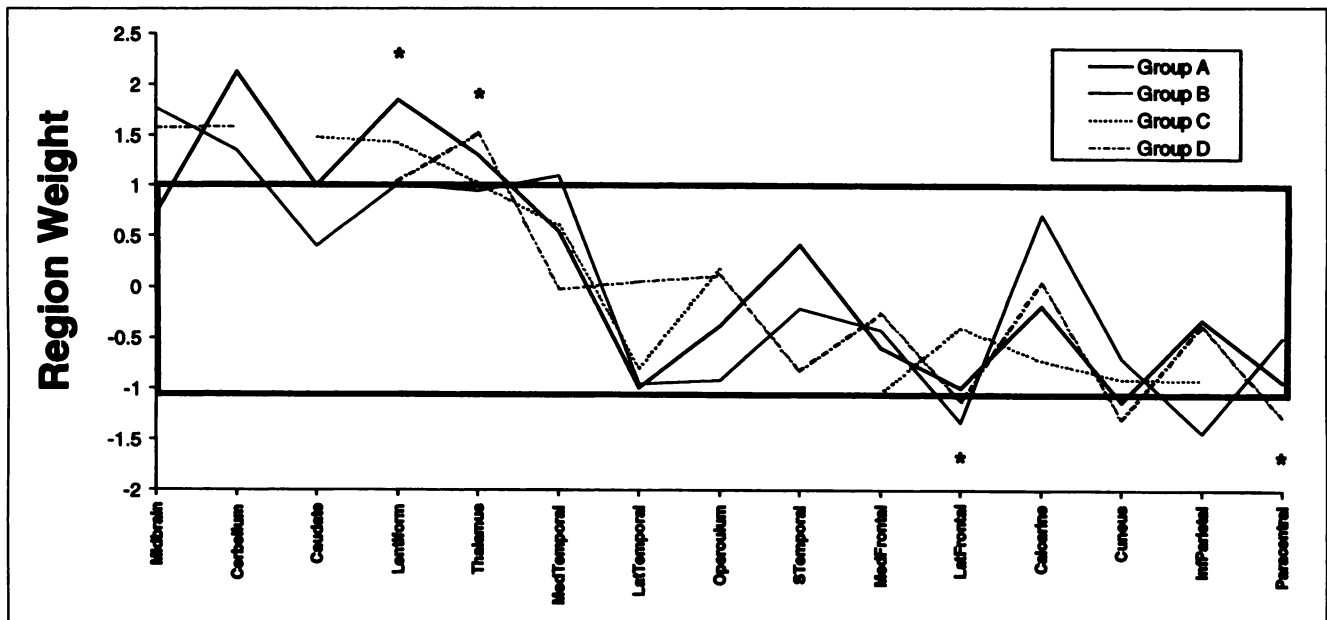


FIGURE 1. Region weights for metabolic covariance patterns associated with PD. Regions having weights with absolute values ≥ 1 (those outside box) contributed significantly to pattern topography, accounting for $>50\%$ of variance in normalized metabolic data ($P < 0.01$, corrected for multiple ROIs). Pattern-related increases in lentiform-thalamic metabolism covaried with relative metabolic decreases in motor cortical regions (*).

Voxel-Based Covariance Analysis

Using voxel-based SSM to analyze the group B images, we identified a disease-related pattern represented by the second principal component of the SSM analysis, accounting for 11% of the subject \times voxel variance (3,4). The topography of this pattern was similar to that identified in the ROI-based analyses (Fig. 3A). Subject scores for this pattern discriminated the PD patients from healthy volunteers ($P < 0.005$) (Fig. 3B). Subject scores for the ROI-based and the voxel-based group B disease-related covariance patterns

were found to be significantly correlated ($r^2 = 0.59$, $P < 0.0001$).

Prospective Discrimination

Subject scores for the group A PDRP were computed prospectively for each member of groups B, C and D, using TPR. In each group, the PDRP scores computed using TPR correlated significantly with the subject scores for the disease-related patterns identified by SSM analysis (group B, ROI analysis: $r^2 = 0.92$; group B, voxel analysis: $r^2 =$

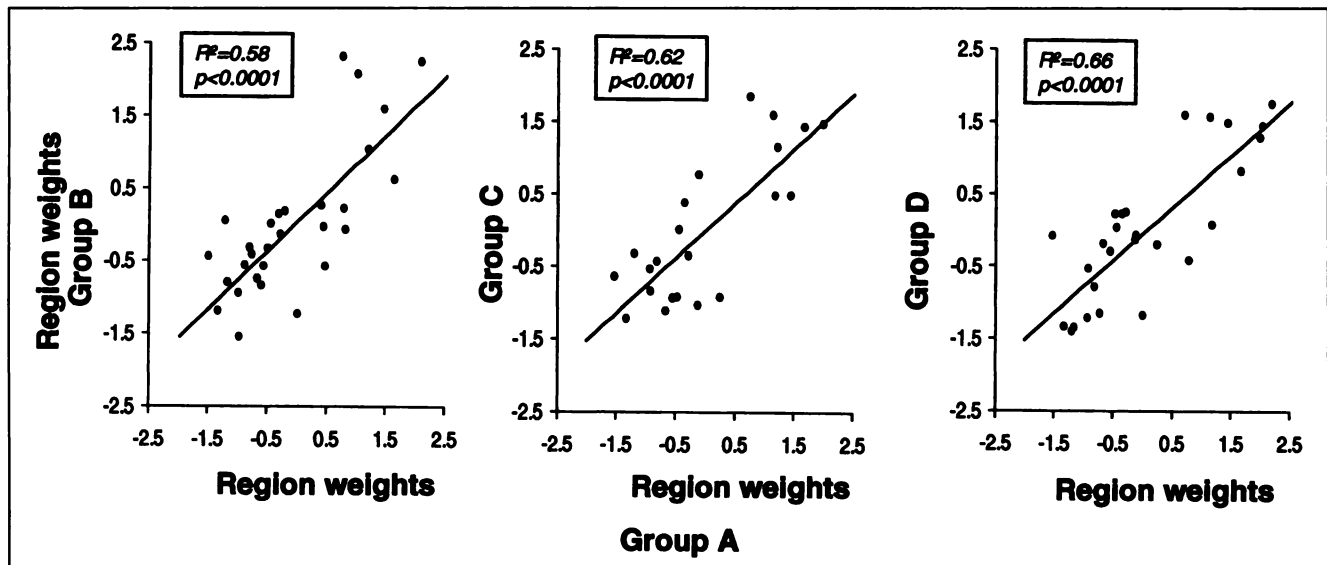


FIGURE 2. Correlations between region weights for group A PDRP seen in Figure 1 and corresponding regional values for disease-related covariance patterns identified in groups B, C and D ($P < 0.0001$).

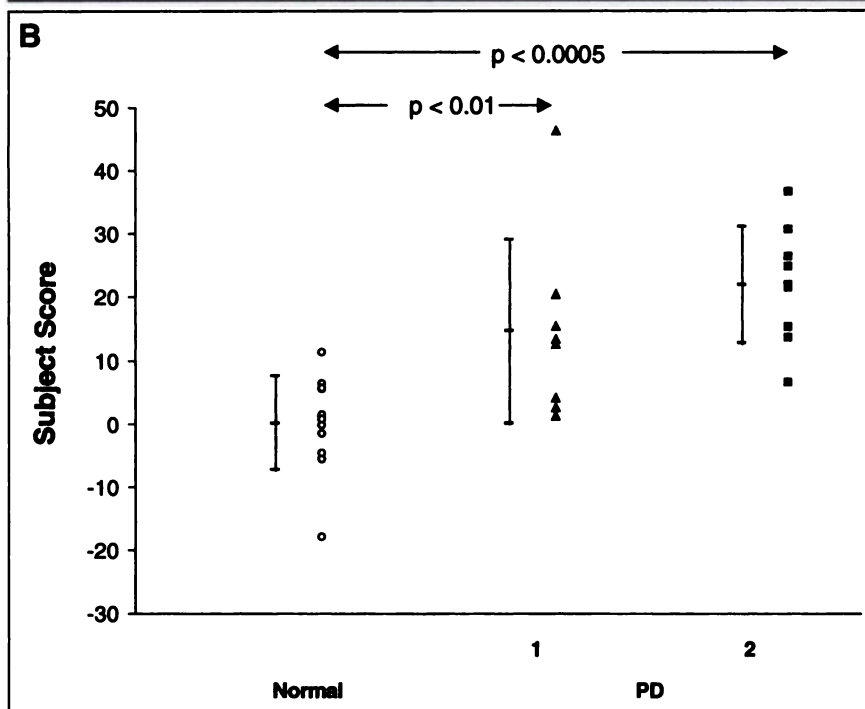
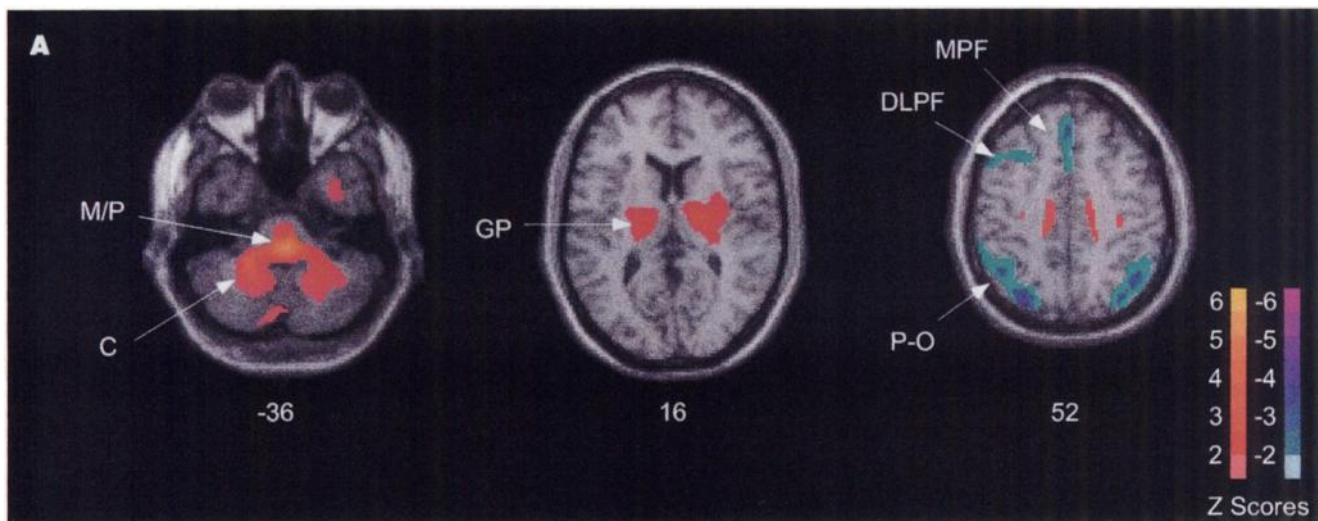


FIGURE 3. (A) Three axial slices taken from whole-brain voxel-based SSM analysis of group B metabolic data show major regions contributing to voxel-derived regional covariance pattern associated with PD. Numbers under each slice are in millimeters relative to anterior-posterior commissural line. Voxels with region weights less than $Z = 1.5$ are color-coded red-yellow, and region weights less than $Z = -1.5$ are color-coded blue-purple. M/P = midbrain/pons; C = cerebellum; GP = globus pallidus; DLPF, dorsolateral prefrontal cortex; MPF = medial prefrontal cortex; P-O = parieto-occipital cortex. (B) Scatter diagram of subject scores for voxel-based PD-related covariance pattern presented in (A). Subject scores for this pattern discriminated between mild and more advanced PD patients (filled triangles and squares, respectively) from healthy volunteers (open circles).

0.59; group C, ROI analysis: $r^2 = 0.62$; group D, ROI analysis: $r^2 = 0.95$; $P < 0.001$ for all correlations). These prospectively computed PDRP subject scores discriminated PD patients from healthy volunteers in all four populations studied ($P < 0.004$) (Fig. 4). Discriminant analysis of the PDRP subject scores for the original group A patients and healthy volunteers was reported previously with between-group differentiation comparable with that of the other populations (4).

DISCUSSION

This study demonstrates that the abnormal regional metabolic covariance patterns associated with PD are highly reproducible across patient populations and tomographs. We used the PDRP previously reported in the group A analysis (4) as a benchmark against which to compare the correspond-

ing disease-related patterns identified in the other populations. Disease-related covariance patterns identified by FDG PET using SSM analysis were topographically similar in the four populations studied. Indeed, region weights for the group A PDRP accounted for approximately 60% of the variation in the region weights for the analogous patterns identified in groups B, C and D. Thus, the disease-related topographies extracted in the SSM analyses of rCMRGlc data from PD patients and healthy volunteers is stable, despite differences in PET instrumentation and image quantification procedures across imaging centers (4,9). Indeed, the unaccounted-for variance in the region weight correlations was similar for each group ($\sim 40\%$), suggesting that the magnitude of these methodological effects is stable across populations and tomographs.

These findings extend those reported previously, in which

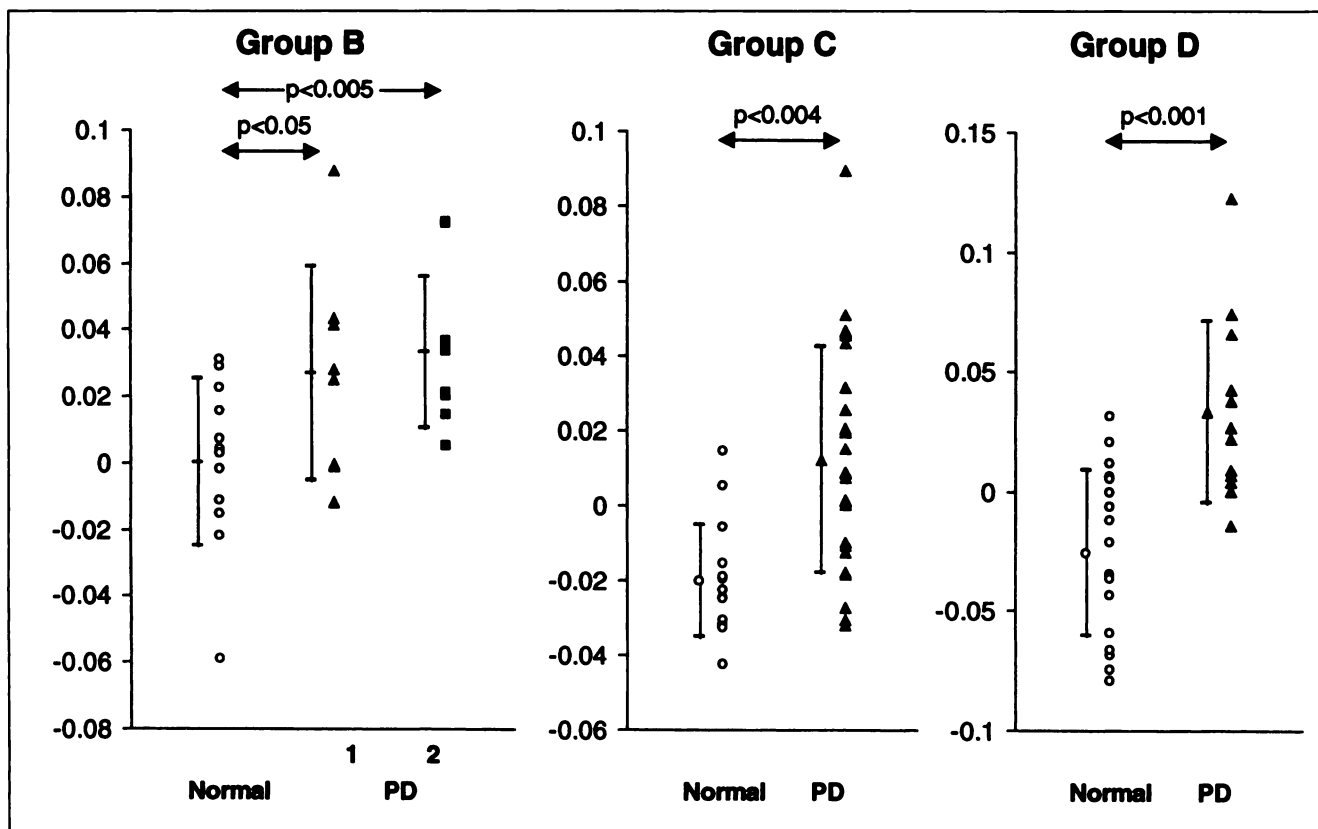


FIGURE 4. Discriminant function analysis of subject scores for group A PDRP computed prospectively for each patient (filled triangle) and healthy volunteer (open circle) in groups B, C and D.

significant region weight correlations were identified for the PDRPs identified in the analyses of data from groups A and D (4,5). This study demonstrates the reproducibility of the group A PDRP in two additional populations: one scanned on another intermediate-resolution tomograph (group C) and another scanned on a new high-resolution tomograph (group B). Indeed, the topographic stability of PDRPs across populations supports the notion of their relationship to the inherent functional anatomy of parkinsonism (4,8,14).

Although the PD patients and the healthy volunteers were closely matched in age in two populations (groups B and C), there was a mean age disparity of approximately one decade in group A and three decades in group D. In spite of the presence of considerable differences in age between patients and healthy volunteers in some of the populations, SSM analysis revealed topographically similar disease-related covariance patterns. We attribute this to the relative independence of the PDRP and the SSM aging patterns identified previously (9). Thus, the normal aging process does not appear to play a major role in the progressive expression of the PDRP that occurs with advancing parkinsonism (10).

We also tested the utility of the group A PDRP as a potential metabolic imaging marker for the diagnosis of PD. By projecting the region weights for this PDRP into the rCMRGlc data from each PD patient and healthy volunteer (7,9,10,15), the expression of this pattern (PDRP subject score) was computed prospectively on an individual basis

for every subject in each of the four populations studied. Indeed, the resulting PDRP scores discriminated PD patients from healthy volunteers in the different groups with comparable accuracy. However, there was some degree of overlap between patients and healthy volunteers that varied across populations. We attribute this to the inclusion of different numbers of early-stage patients in each group. In contrast to the striatal uptake of FDOPA or radiolabeled cocaine derivatives (19–21), PDRP expression increases, rather than decreases, with disease progression. Thus, this metabolic marker may be somewhat less sensitive at early stages of disease (4). Nonetheless, we have found that reliable early differential diagnosis can be achieved with FDG PET through the use of covariance patterns of regional metabolic asymmetries (4,5,11). Subject scores for these patterns are often elevated with early stage disease and may be used to differentiate typical and atypical parkinsonism at or near the time of clinical onset (11). Interestingly, in this study, we found a significant increase in PDRP subject scores in the 10 Hoehn and Yahr stage I patients comprising group B1. Thus, with improved PET instrumentation, it may be possible to differentiate early-stage patients from healthy volunteers without applying adjunctive asymmetry analyses. Additional FDG PET studies of independent cohorts or Hoehn and Yahr stage I patients will be needed to assess the comparative utility of the PDRP and the metabolic asymmetries topographies in early-stage differential diagnosis.

Our results demonstrated that the PD-related topographies identified using ROI-based SSM analysis were reproducible across the four populations studied. In addition, in group B subjects, imaged on a PET instrument with a field of view sufficient to include the whole brain, we found that a topographically similar PD-related covariance pattern could also be identified using a voxel-based SSM approach. Indeed, within subjects in that cohort, the individual expression of the disease-related patterns identified in the voxel-based SSM analyses correlated significantly ($r^2 \sim 0.60$), with corresponding values for the ROI-based pattern scores. Moreover, the subject scores for the voxel-based and the ROI-based disease-related patterns afforded comparable degrees of discrimination between the patient and healthy volunteer groups. Thus, the delineation of SSM markers for brain disorders such as PD is not necessarily restricted to ROI data and can be applied using fully automated voxel-based methods. Nonetheless, the reproducibility of voxel-based disease topographies across populations and tomographs is a topic for further investigation.

CONCLUSION

This study demonstrates a high degree of reproducibility of the PDRPs identified in resting-state FDG PET data, despite differences in PET instrumentation and quantification procedures. The topography of these patterns is consistent with abnormal patterns of functional connectivity evident in both experimental animal models and in human subjects (4,8,14). Moreover, FDG PET imaging is comparatively simple and widely available. Thus, the computation of PDRP subject scores in individual patients may have significant clinical utility in the differential diagnosis and objective assessment of disease progression in parkinsonism.

ACKNOWLEDGMENTS

This study was supported by National Institutes of Health grant NSRO135069 and by generous grants from the National Parkinson Foundation and the Parkinson Disease Foundation. David Eidelberg is a Cotzias Fellow of the American Parkinson Disease Association. We acknowledge the important contributions of Drs. Phoebe Spetsieris and Thomas Chaly to this work. We thank Claude Margouleff for help with the PET studies, Dr. Robert Dahl and Ralph

Matacchieri for cyclotron support and Jennifer Mazurkiewicz for manuscript preparation.

REFERENCES

1. Moeller JR, Strother SC, Sidtis JJ, Rottenberg DA. The scaled subprofile model: a statistical approach to the analysis of functional patterns in positron emission tomographic data. *J Cereb Blood Flow Metab.* 1987;7:649–658.
2. Moeller JR, Strother SC. A regional covariance approach to the analysis of functional patterns in positron emission tomographic data. *J Cereb Blood Flow Metab.* 1991;11:A121–A135.
3. Alexander GE, Moeller JR. Application of the scaled subprofile model to functional imaging in neuropsychiatric disorders: principal component approach to modeling brain function in disease. *Hum Brain Mapping.* 1994;2:1–16.
4. Eidelberg D, Moeller JR, Dhawan V, et al. The metabolic topography of parkinsonism. *J Cereb Blood Flow Metab.* 1994;14:783–801.
5. Eidelberg D, Moeller JR, Dhawan V, et al. The metabolic anatomy of Parkinson's disease: complementary ^{18}F -fluorodeoxyglucose and ^{18}F -fluorodopa PET studies. *Mov Disord.* 1990;5:203–213.
6. Fahn S, Elton RL, and the UPDRS Development Committee. Unified Parkinson disease rating scale. In: Fahn S, Marsden CD, Calne D, Goldstein M, eds. *Recent Developments in Parkinson's Disease.* Vol 2. Floral Park, NJ: Macmillan; 1984:293–304.
7. Eidelberg D, Moeller JR, Ishikawa T, et al. The assessment of disease severity in parkinsonism with ^{18}F -fluorodeoxyglucose and PET. *J Nucl Med.* 1995;36:378–383.
8. Eidelberg D, Moeller JR, Ishikawa T, et al. Regional metabolic correlates of surgical outcome following unilateral pallidotomy for Parkinson's disease. *Ann Neurol.* 1996;39:450–459.
9. Moeller JR, Ishikawa T, Dhawan V, et al. The metabolic topography of normal aging. *J Cereb Blood Flow Metab.* 1996;16:385–398.
10. Moeller JR, Eidelberg D. Divergent expression of regional metabolic topographies in Parkinson's disease and normal aging. *Brain.* 1997;120:2197–2206.
11. Eidelberg D, Moeller JR, Ishikawa T, et al. Early differential diagnosis of Parkinson's disease with ^{18}F -fluorodeoxyglucose and PET. *Neurology.* 1995;45:1995–2004.
12. Robeson W, Dhawan V, Babchick B, et al. SuperPETT 3000 time-of-flight tomograph: optimization of factors affecting quantification. *IEEE Trans Nucl Sci.* 1993;40:135–142.
13. De Grado TR, Turkington TG, Williams JJ, Stearns CW, Hoffman JM, Coleman RE. Performance characteristics of a whole-body PET scanner. *J Nucl Med.* 1994;35:1398–1406.
14. Eidelberg D, Moeller JR, Kazumata K, et al. Metabolic correlates of pallidal neuronal activity in Parkinson's disease. *Brain.* 1997;120:1315–1324.
15. Antonini A, Moeller JR, Nakamura T, et al. The metabolic anatomy of tremor in Parkinson's disease. *Neurology.* 1998;51:803–810.
16. Antonini A, Leenders KL, Spiegel R, et al. Striatal glucose metabolism and dopamine D_2 receptor binding in asymptomatic gene carriers and patients with Huntington's disease. *Brain.* 1996;119:2085–2095.
17. Kearfott KJ, Carroll LR. Evaluation of the performance characteristics of the PC4600 positron emission tomograph. *J Comput Assist Tomogr.* 1984;8:502–513.
18. Friston KJ, Holmes AP, Worsley KJ, et al. Statistical parametric maps in functional neuroimaging: a general linear approach. *Hum Brain Mapping.* 1995;2:189–210.
19. Ishikawa T, Dhawan V, Chaly T, et al. Clinical significance of striatal dopa decarboxylase activity in Parkinson's disease. *J Nucl Med.* 1996;37:216–222.
20. Ishikawa T, Dhawan V, Kazumata K, et al. Comparative nigrostriatal dopaminergic imaging with ^{123}I]βCIT-FP/SPECT and ^{18}F]FDOPA/PET. *J Nucl Med.* 1996;37:1760–1765.
21. Kazumata K, Dhawan V, Chaly T, et al. Dopamine transporter imaging with fluorine-18-FPCIT and PET. *J Nucl Med.* 1998;39:1521–1530.